PERGAMON

International Journal of Heat and Mass Transfer 44 (2001) 4401–4411

International Journal of HEAT and MASS TRANSFER

www.elsevier.com/locate/ijhmt

Analysis of non-Darcian effects on temperature differentials in porous media

A. Marafie, K. Vafai *

Department of Mechanical Engineering, The Ohio State University, Columbus, OH 43210, USA

Received 30 June 2000; received in revised form 8 March 2001

Abstract

Forced convection flow through a channel filled with a porous medium is investigated analytically. A non-thermal equilibrium, two-equation model is utilized to represent the fluid and solid energy transport. The Darcy–Forchheimer–Brinkman model is used to represent the fluid transport within the porous medium. Analytical solutions are obtained for both fluid and solid temperature fields incorporating the effects of various pertinent parameters such as the Biot number, the thermal conductivity ratio, the Darcy number and the inertial parameter. The present analytical solution for the two-equation model is validated against the exact solution for the one-equation model available in the literature as well as the analytical solution for the non-thermal equilibrium case based on a Darcian flow field. Error maps for the validity of one-equation model are established for various physical conditions taking into account the Darcy and inertial parameters as well as the Biot and the thermal conductivity ratio of fluid to solid phases. It is shown that the Darcy number and the inertial parameter have a lesser influence in establishing the validity of the local thermal equilibrium assumption.

Keywords: Porous media; Local thermal non-equilibrium; Forced convection; Non-Darcian effects

1. Introduction

Forced convective heat transfer in porous media has been the subject of many recent studies due to numerous practical applications such as nuclear waste repository, energy storage units, electronic cooling, thermal insulation, packed bed heat exchangers, heat pipes, drying technology, catalytic reactors, petroleum industries and geothermal systems. The assumption of local thermal equilibrium is widely used in many of these applications. However, this assumption breaks down when a substantial temperature difference exists between the solid and the fluid phases. More recently, local thermal non-equilibrium has received considerable attention due to its pertinence in applications where such a temperature differential exists between the solid and the fluid phases.

The work of Vafai and Tien [1] was one of the early attempts to account for the boundary and inertia effects in the momentum equation for a porous medium. They found that the momentum boundary layer thickness is of the order of $\sqrt{K/\varepsilon}$. Vafai and Thiyagaraja [2] presented analytical solutions for the velocity and temperature fields for the interface region using the Brinkman–Forchheimer–extended Darcy equation. They considered three fundamental types of the interface namely, the interface between two porous media, the interface between a porous medium and a fluid layer and the interface between a porous medium and an impermeable medium. Amiri and Vafai [3] employed a general fluid flow model and a two-phase energy equation to investigate the forced convective heat transfer within a channel with constant wall temperature. They included the effects of variable porosity and thermal dispersion in their analysis and error maps for assessing the importance of various simplifying assumptions that are commonly used were established in their work.

Lee and Vafai [4] employed the non-thermal equilibrium model to investigate the forced convective flow

* Corresponding author. Present address. Department of Mechanical Engineering, University of California, A363 Bourns Hall, Riverside, CA 92521-0425, USA. Tel.: +1-909-787-2135; fax: +1-909-787-2899.

E-mail address: vafai@engr.ucr.edu (K. Vafai).

0017-9310/01/$ - see front matter
PII: S0017-9310(01)00099-0

Nomenclature

a	interfacial area per unit volume of porousmedia (m^{-1})
Bi	Biot number defined by Eq. (21)
c_p	specific heat of the fluid (J kg^{-1} K^{-1})
D_h	hydraulic diameter of the channel (m)
Da	Darcy number defined by Eq. (14)
E	error in the Nusselt number defined by Eq. (67)
F	a function that depends on the Reynolds number and the microstructure of the porous medium, used to express the inertia term
h_i	interstitial heat transfer coefficient (W m^{-2} K^{-1})
h_{w1}	wall heat transfer coefficient for the one-equation model defined by Eq. (63)) (W m^{-2} K^{-1})
h_{w2}	wall heat transfer coefficient for the two-equation model defined by Eq. (57) (W m^{-2} K^{-1})
H	characteristic length of the channel (m)
K	permeability of the porous medium (m^2)
$k_{f,eff}$	effective thermal conductivity of the fluid (W m^{-1} K^{-1})
$k_{s,eff}$	effective thermal conductivity of the solid (W m^{-1} K^{-1})
Nu_{w1}	Nusselt number for the one-equation model defined by Eq. (64)
Nu_{w2}	Nusselt number for the two-equation model defined by Eq. (58)
P	pressure (N m^{-2})
q_w	heat flux at the wall (W m^{-2})
Re	Reynolds number defined by Eq. (29)
T	temperature (K)
u	longitudinal velocity of the fluid (m s^{-1})
u_∞	longitudinal velocity outside the momentum boundary layer
u^*	non-dimensional longitudinal velocity defined by Eq. (10)
x	longitudinal coordinate (m)
y	transverse coordinate (m)

Greek symbols

α_e	effective thermal diffusivity $= k_e/\rho_f c_p$(m^2 s^{-1})
η	non-dimensional transverse coordinate defined by Eq. (10)
γ	geometric constant defined by Eq. (11)
κ	ratio of the effective fluid conductivity to that of the solid defined by Eq. (22)
θ	non-dimensional temperature defined by Eq. (10)
θ_b	non-dimensional bulk mean temperature defined by Eq. (66)
$\theta_{f,b}$	non-dimensional fluid bulk mean temperature defined by Eq. (60)
ξ	non-dimensional longitudinal coordinate defined by Eq. (27)
δ	porosity of the porous media
Λ	inertia parameter defined by Eq. (15)
μ_f	fluid viscosity (kg m^{-1} s^{-1})
ν_f	fluid kinematic viscosity (m^2 s^{-1})
ρ_f	fluid density (kg m^{-3})
β	constant defined by Eq. (28)

Subscripts/superscripts

f	fluid phase
s	solid phase
w	wall
*	non-dimensional
eff	effective property

Other symbol

$\langle\rangle$	'local volume average' of a quantity

through a channel filled with a porous medium subject to a constant heat flux. They obtained analytical solutions for the fluid and solid phase temperature distributions. In their work, the validity of the one-equation model was presented, considering a Darcian fluid flow. Kim et al. [5] presented an analytical solution for the two-equation model including the boundary effect for an equivalent microchannel application. They presented analytical solutions for the fluid and solid phase temperature distributions based on the Brinkman-extended Darcy equation. They also analyzed the validity of the local thermal equilibrium assumption. Vafai and Kim [6] presented an exact solution for fully developed flow in a porous channel bounded by parallel plates subject to constant heat flux boundary conditions. Kuznetsov [7] obtained an interesting analytical solution for the temperature difference between the solid and liquid phases for the problem of thermal non-equilibrium in a parallel plate channel with constant heat flux using a perturbation approach. However, his analysis could not produce a temperature distribution for any of the phases, nor could it lead to a Nusselt number or an error map configuration.

In the present work, analytical expressions for the fluid and solid phase temperature distributions are obtained for convective flow through the channel with a constant heat flux applied at walls and accounting for both boundary and inertial effects. To this end, the Brinkman–Forchhiemer–extended Darcy equation, which accounts for boundary and inertia effects, is used to obtain the velocity field. Errors maps characterizing validity of the thermal equilibrium are obtained for a

range of Darcy and inertia numbers and the non-Darcian effects on temperature differentials in porous media are established.

2. Modeling and formulation

2.1. Problem description

The schematic diagram of the problem is shown in Fig. 1. A rectangular channel or a circular duct is filled with porous medium and is subject to a constant heat flux boundary condition. The height of the channel or the diameter of the circular duct is 2H. Due to symmetry considerations, one half of the channel is considered. The following assumptions are invoked:

1. Negligible radiation and natural convection.
2. Constant thermophysical properties.
3. Fully developed fluid flow and heat transfer conditions.

2.2. Mathematical modeling

2.2.1. Governing equations

The momentum equation, accounting for the inertia and boundary effects, is given by Vafai and Tien [1]

$$\frac{\mu_f}{\delta}\nabla_y^2\langle u\rangle - \frac{\mu_f}{K}\langle u\rangle - \rho_f F\frac{\delta}{K^{1/2}}\langle u\rangle^2 - \frac{\mathrm{d}\langle P\rangle^f}{\mathrm{d}x} = 0. \tag{1}$$

The energy equations for the solid and fluid phase are based on the work of Amiri and Vafai [3] employing a non-thermal equilibrium model.

Fluid phase:

$$k_{f,\mathrm{eff}}\nabla_y^2\langle T_f\rangle^f + h_i a\left(\langle T_s\rangle^s - \langle T_f\rangle^f\right) = \rho c_p\langle u\rangle\frac{\partial\langle T_f\rangle^f}{\partial x}. \tag{2}$$

Solid phase:

$$k_{s,\mathrm{eff}}\nabla_y^2\langle T_s\rangle^s - h_i a\left(\langle T_s\rangle^s - \langle T_f\rangle^f\right) = 0. \tag{3}$$

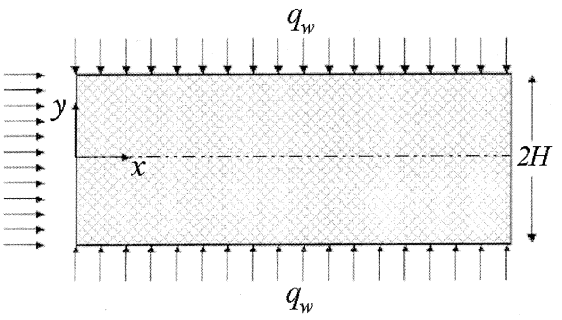

Fig. 1. Schematic of the physical model for flow through a rectangular channel or a ciruclar duct and the coordinate system.

The net transverse conduction is represented by the first term of the above two equations, while the axial conduction is dropped since its contribution to the net energy transfer is not significant [3]. Physical aspects of the above equations are discussed in Lee and Vafai [4] and Bejan [8]. Furthermore, a comprehensive analysis of the variances among different models and the dispersion and variable porosity effects are presented in Alazimi and Vafai [9]. Two basic geometries are considered. These are a rectangular channel and a circular duct. As such, the term $\nabla_y^2\langle\rangle$ is represented by:

$$\nabla_y^2\langle\rangle = \frac{\partial^2\langle\rangle}{\partial y^2} \quad \text{(Rectangular channel)}, \tag{4}$$

$$\nabla_y^2\langle\rangle = \frac{1}{y}\frac{\partial}{\partial y}\left(y\frac{\partial\langle\rangle}{\partial y}\right) \quad \text{(Circular duct)}. \tag{5}$$

The second term represents the local interaction between the fluid and solid and the last term in the fluid's energy equation describes the convective energy transfer.

2.2.2. Boundary conditions

The fluid boundary conditions are represented by:

$$\left.\frac{\mathrm{d}\langle u\rangle}{\mathrm{d}y}\right|_{y=0} = 0, \quad \langle u\rangle|_{y=H} = 0. \tag{6}$$

By choosing a boundary with a high thermal conductivity, the temperature of the solid and the fluid at the wall interface will be the same,

$$\langle T_f\rangle^f\Big|_{y=H} = \langle T_s\rangle^s|_{y=H} = T_w. \tag{7}$$

Another representation of the boundary condition is found by noting the following. The amount of heat flux applied at the wall will be divided between the two phases based on their effective thermal conductivity and temperature gradient as set below,

$$q_w = k_{f,\mathrm{eff}}\left.\frac{\partial\langle T_f\rangle}{\partial y}\right|_{y=H} + k_{s,\mathrm{eff}}\left.\frac{\partial\langle T_s\rangle}{\partial y}\right|_{y=H} \tag{8}$$

and the symmetry condition at the center of the channel can be written as

$$\left.\frac{\partial\langle T_f\rangle^f}{\partial y}\right|_{y=0} = \left.\frac{\partial\langle T_s\rangle^f}{\partial y}\right|_{y=0} = 0. \tag{9}$$

2.2.3. Normalization

The following dimensionless variables are introduced for normalizing the governing equations and boundary conditions

$$u^* = \frac{\langle u\rangle}{u_\infty}, \quad \eta = \frac{y}{H}, \quad \theta = \gamma\frac{k_{s,\mathrm{eff}}(\langle T\rangle - T_w)/H}{q_w}. \tag{10}$$

In the above equations, γ is a geometric constant depending on the channel cross-section geometry and is represented by

$$\gamma = \frac{D_h}{4H}, \tag{11}$$

where D_h is the hydraulic diameter of the channel. For a rectangular cross-section channel $\gamma = 1$ while for a circular cross-section channel $\gamma = 1/2$.

Adding Eqs. (2) and (3), integrating it over the channel cross-section and applying boundary conditions (8) and (9) results

$$\rho c_p \langle u \rangle \frac{\partial \langle T_f \rangle^f}{\partial x} = \frac{q_w}{\gamma H}. \tag{12}$$

The non-dimensional momentum equation can be written as

$$\nabla_y^2 u - \frac{u}{Da} - \frac{\Lambda}{\sqrt{Da}} u^2 - \frac{1}{Da}\frac{1}{u_\infty}\frac{K}{\mu_f}\frac{d\langle P \rangle^f}{dx} = 0, \tag{13}$$

where the * superscript has been dropped for convenience and the Darcy number and inertia parameter are defined as:

$$Da = \frac{K}{H^2 \delta}, \tag{14}$$

$$\Lambda = \frac{\delta^{3/2} F u_\infty H}{\nu_f}. \tag{15}$$

The non-dimensional boundary conditions for the momentum equation are

$$\left.\frac{du}{dy}\right|_{\eta=0} = 0, \quad u|_{\eta=1} = 0. \tag{16}$$

Utilizing Eqs. (10) and (12), the energy equations and the associated boundary conditions can be written as:

$$\kappa \nabla_\eta^2 \theta_f + \frac{1}{\gamma} Bi(\theta_s - \theta_f) = u, \tag{17}$$

$$\nabla_\eta^2 \theta_s - \frac{1}{\gamma} Bi(\theta_s - \theta_f) = 0, \tag{18}$$

$$\theta_s(1) = \theta_f(1) = 0, \tag{19}$$

$$\theta_s'(0) = \theta_f'(0) = 0, \tag{20}$$

where the κ is the ratio of the effective thermal conductivity of the fluid to solid and Bi is the Biot number which represents the ratio of the internal convection heat transfer between the solid and fluid to the conduction resistance of the solid, represented by:

$$Bi = \frac{h_i \gamma a H^2}{k_{s,eff}}, \tag{21}$$

$$\kappa = \frac{k_{f,eff}}{k_{s,eff}}. \tag{22}$$

In this work, the temperature distributions for the solid and fluid phases are presented for the case of a rectangular channel.

2.3. Analysis

2.3.1. Velocity profile

Vafai and Thiyagaraja [2] had derived an analytical expression for the velocity distribution for flow over an external boundary using a singular perturbation analysis, for the case of interface region between a porous medium and an impermeable medium. After some modifications, to adopt their result for the case of internal flow within a channel, yields the following velocity distribution

$$u(\xi) = (u^0(\xi) + \delta u^1(\xi) + \delta^2 u^2(\xi) + \cdots) \times (1 + \Lambda\sqrt{Da}), \tag{23}$$

where

$$u^0(\xi) = 1 - \exp(-\xi), \tag{24}$$

$$u^1(\xi) = \beta\left[-1 + \exp(-\xi)\left(\frac{2}{3} + \xi\right) + \frac{1}{3}\exp(-2\xi)\right], \tag{25}$$

$$u^2(\xi) = \beta^2\left[2 + \frac{1}{2}\exp(-\xi)\left(\xi^2 - \frac{13}{3}\xi - \frac{29}{18}\right) - \frac{1}{3}\exp(-2\xi)\left(2\xi + \frac{10}{3}\right) - \frac{1}{12}\exp(-3\xi)\right] \tag{26}$$

and where

$$\xi = \frac{1-\eta}{\sqrt{Da}}, \tag{27}$$

$$\beta = F Re, \tag{28}$$

$$Re = \frac{\Lambda\sqrt{Da}}{\delta F}(1 + \Lambda\sqrt{Da}). \tag{29}$$

In the above equations, δ is the porosity of the porous medium, Re, the Reynolds number and F is a function used to express the inertia term that depends on the Reynolds number and the microstructure of the porous medium.

2.3.2. Temperature distribution

Utilizing the two coupled energy equations, Eqs. (17) and (18) which contain two unknowns, the following equations can be obtained for the fluid and solid dimensionless temperatures.

$$\kappa\theta_f''''(\eta) - Bi(1+\kappa)\theta_f''(\eta) = -Biu\left(\frac{1-\eta}{\sqrt{Da}}\right) + u''\left(\frac{1-\eta}{\sqrt{Da}}\right), \tag{30}$$

$$\kappa\theta_s''''(\eta) - Bi(1+\kappa)\theta_s''(\eta) = -Biu\left(\frac{1-\eta}{\sqrt{Da}}\right). \tag{31}$$

Two more sets of boundary conditions are required to solve the above fourth-order differential equations. These are obtained by applying the boundary conditions

given in Eqs. (19) and (20) to Eqs. (17) and (18). This results in

$$\theta_s''(1)=0,\quad \theta_f''(1)=\frac{u(\eta=1)}{\kappa}=\frac{u_1}{\kappa}, \tag{32}$$

$$\theta_s'''(0)=0,\quad \theta_f'''(0)=\frac{u'(\eta=0)}{\kappa}=\frac{u_0'}{\kappa}, \tag{33}$$

where $u_1=u(\eta=1)$ and $u_0'=u'(\eta=0)$. The temperature distribution is found by solving Eqs. (30) and (31) and applying the boundary conditions given by Eqs. (19), (20), (32) and (33). After a lengthy process this results in

$$\theta_s(\eta)=2\frac{\sum_{i=1}^{2}\Gamma_i(\eta)}{\alpha_1}-\frac{\mu}{2\alpha_1}\eta^2+\frac{C_1}{\alpha_1^2}\cosh(\alpha_1\eta)+C_2\eta \tag{34}$$

and

$$\theta_f(\eta)=2\frac{\sum_{i=1}^{4}\Gamma_i(\eta)}{\alpha_1}-\frac{\mu}{2\alpha_1}\eta^2+\frac{C_3}{\alpha_1^2}\sinh(\alpha_1\eta)+\frac{C_4}{\alpha_1^2}\times\cosh(\alpha_1\eta)+C_5, \tag{35}$$

where

$$\alpha_1=\sqrt{\frac{(1+\kappa)Bi}{\kappa}}, \tag{36}$$

$$\mu=\frac{\alpha_2(1-\delta\beta+2\delta^2\beta^2)}{\alpha_1}, \tag{37}$$

$$\alpha_2=\frac{-Bi(1+\Lambda\sqrt{Da})}{\kappa}, \tag{38}$$

$$C_1=\frac{1}{\alpha_1}[-\Lambda_{1s}(1)\tanh(\alpha_1)+\Lambda_{2s}(1)], \tag{39}$$

$$C_2=-2\frac{\sum_{i=1}^{2}\Gamma_i(1)}{\alpha_1}+\frac{\mu}{2\alpha_1}-\frac{C_1}{\alpha_1^2}\cosh(\alpha_1), \tag{40}$$

$$C_3=\frac{u_0'}{\kappa\alpha_1}, \tag{41}$$

$$C_4=\frac{u_1}{\kappa\cosh(\alpha_1)}-\frac{1}{\alpha_1}[(\Lambda_{1s}(1)+\Lambda_{1f}(1)+C_4\alpha_1)\tanh(\alpha_1)+(-\Lambda_{2s}(1)+\Lambda_{2f}(1))], \tag{42}$$

$$C_5=-2\frac{\sum_{i=1}^{4}\Gamma_i(1)}{\alpha_1}+\frac{\mu}{2\alpha_1}-\frac{C_3}{\alpha_1^2}\sinh(\alpha_1)-\frac{C_4}{\alpha_1^2}\cosh(\alpha_1) \tag{43}$$

and

$$\begin{aligned}\Gamma_i(\eta)=&\gamma_{i1}[\cosh(B_7)+\sinh(B_7)]+\gamma_{i2}[(B_7\cosh(B_7)-2\sinh(B_7))+(B_7\sinh(B_7)-2\cosh(B_7))]\\&+\gamma_{i3}[(B_7^2\cosh(B_7)-4B_7\sinh(B_7)+6\cosh(B_7))+(B_7^2\sinh(B_7)-4B_7\cosh(B_7)+6\sinh(B_7))]\\&+\gamma_{i4}[\cosh(2B_7)+\sinh(2B_7)]\\&+\gamma_{i5}[(2B_7\cosh(2B_7)-2\sinh(2B_7))+(2B_7\sinh(2B_7)-2\cosh(2B_7))]\\&+\gamma_{i6}[\cosh(3B_7)+\sinh(3B_7)],\end{aligned} \tag{44}$$

where

$$\begin{aligned}\gamma_{i1}&=\frac{1}{D^2}\left[\lambda_{i1}\left(\frac{(-1)^{i+1}}{2}\right)-\frac{\lambda_{i2}}{2}\left((-1)^{i+1}+\alpha_1\right)+\lambda_{i3}\left((-1)^{i+1}\frac{\alpha_1^2}{2}+\alpha_1+(-1)^{i+1}\right)\right],\\ \gamma_{i2}&=\frac{(-1)^{i+1}}{D^2}\left((-1)^{i+1}-\frac{\alpha_1}{D}\right)\left[\lambda_{i2}\left(\frac{(-1)^{i+1}}{2}\right)-\lambda_{i3}\left((-1)^{i+1}+\alpha_1\right)\right],\\ \gamma_{i3}&=\frac{1}{D^2}\left[\lambda_{i3}\left((-1)^{i+1}\frac{\alpha_1^2}{2D^2}-\frac{\alpha_1}{D}+\frac{(-1)^{i+1}}{2}\right)\right],\\ \gamma_{i4}&=\frac{1}{8D^2}\left[\lambda_{i4}(-1)^{i+1}-\lambda_{i5}\left((-1)^{i+1}+\alpha_1\right)\right],\\ \gamma_{i5}&=\frac{1}{8D^2}\left[\lambda_{i5}\left((-1)^{i+1}-\frac{\alpha_1}{2D}\right)\right],\\ \gamma_{i6}&=\frac{1}{18D^2}\left[\lambda_{i6}(-1)^{i+1}\right],\end{aligned} \tag{45}$$

in which,

$$D=\frac{1}{\sqrt{Da}} \tag{46}$$

and

$$\begin{aligned}\lambda_{k1}&=\frac{1}{\beta_i}\left[\mu_{j1}+\frac{\mu_{j2}}{\beta_i}+\frac{\mu_{j3}}{\beta_i^2}\right],\\ \lambda_{k2}&=\frac{1}{\beta_i^2D}\left[\mu_{j2}+\frac{2\mu_{j3}}{\beta_i}\right],\\ \lambda_{k3}&=\frac{1}{\beta_i^3D^2}\mu_{j3},\\ \lambda_{k4}&=\frac{1}{\beta_{i+2}}\left[\mu_{j4}+\frac{\mu_{j5}}{2D}\right],\\ \lambda_{k5}&=\frac{1}{\beta_{i+2}^2D}\left[\frac{\mu_{j5}}{2}\right],\\ \lambda_{k6}&=\frac{1}{\beta_{i+4}}\mu_{j6}.\end{aligned}$$

$$\begin{aligned}&\text{For } k=1 \quad \text{set } i=1,\ j=1, \quad k=2 \quad \text{set } i=2,\ j=1,\\ &\text{For } k=3 \quad \text{set } i=1,\ j=2, \quad k=4 \quad \text{set } i=2,\ j=2,\end{aligned} \tag{47}$$

where the values of k are set through the running summation index in Eq. (43) and

$$
\begin{aligned}
\mu_{11} &= \alpha_2\left[\left(-\frac{29}{72}-\frac{13D}{12}+\frac{D^2}{4}\right)\delta^2\beta^2 + \left(\frac{1}{3}+\frac{D}{2}\right)\delta\beta-\frac{1}{2}\right],\\
\mu_{12} &= \alpha_2 D\left[\left(\frac{13}{12}-\frac{D}{2}\right)\delta^2\beta^2D^2-\frac{1}{2}\delta\beta D^2\right],\\
\mu_{13} &= \alpha_2\left[\frac{1}{4}\delta^2\beta^2D^4\right],\\
\mu_{14} &= \alpha_2\frac{\delta\beta}{3}\left[-\left(D+\frac{5}{3}\right)\delta\beta+\frac{1}{2}\right],\\
\mu_{15} &= \alpha_2\left[\frac{2}{3}\delta^2\beta^2D^2\right],\\
\mu_{16} &= \alpha_2\left[-\frac{1}{24}\delta^2\beta^2\right]
\end{aligned}
\tag{48}
$$

and

$$
\begin{aligned}
\mu_{21} &= \alpha_3\left[\left(-\frac{163}{72}+\frac{25D}{12}-\frac{D^2}{4}\right)\delta^2\beta^2 + \left(\frac{2}{3}-\frac{D}{2}\right)\delta\beta+\frac{1}{2}\right],\\
\mu_{22} &= \alpha_3\left[\left(-\frac{25}{12}+\frac{D}{2}\right)\delta^2\beta^2D^2+\frac{1}{2}\delta\beta D^2\right],\\
\mu_{23} &= \alpha_3\left[-\frac{1}{4}\delta^2\beta^2D^4\right],\\
\mu_{24} &= \alpha_3\left[\left(\frac{4D}{3}+\frac{8}{9}\right)\delta^2\beta^2-\frac{2}{3}\delta\beta\right],\\
\mu_{25} &= \alpha_3\left[-\frac{8}{3}\delta^2\beta^2D^2\right],\\
\mu_{26} &= \alpha_3\left[\frac{3}{8}\delta^2\beta^2\right],
\end{aligned}
\tag{49}
$$

where

$$
\alpha_3 = \frac{-D^2(1+\Lambda\sqrt{Da})}{\kappa} \tag{50}
$$

and where

$$
\begin{aligned}
\beta_1 &= (-\alpha_1+D),\\
\beta_2 &= (\alpha_1+D),\\
\beta_3 &= (-\alpha_1+2D),\\
\beta_4 &= (\alpha_1+2D),\\
\beta_5 &= (-\alpha_1+3D),\\
\beta_6 &= (\alpha_1+3D)
\end{aligned}
\tag{51}
$$

and

$$
\begin{aligned}
B_1 &= \beta_1\eta-D,\\
B_2 &= \beta_2\eta-D,\\
B_3 &= \beta_3\eta-2D\\
B_4 &= \beta_4\eta-2D,\\
B_5 &= \beta_5\eta-3D\\
B_6 &= \beta_6\eta-3D,\\
B_7 &= \eta D-D
\end{aligned}
\tag{52}
$$

and

$$
\begin{aligned}
\Lambda_{1s}(\eta) &= \Lambda_1(\eta)+\Lambda_2(\eta)+\mu\sinh(\alpha_1\eta),\\
\Lambda_{2s}(\eta) &= -\Lambda_1(\eta)+\Lambda_2(\eta)+\mu\cosh(\alpha_1\eta),
\end{aligned}
\tag{53}
$$

$$
\begin{aligned}
\Lambda_{1f}(\eta) &= \Lambda_3(\eta)+\Lambda_4(\eta),\\
\Lambda_{2f}(\eta) &= -\Lambda_3(\eta)+\Lambda_4(\eta),
\end{aligned}
\tag{54}
$$

where

$$
\begin{aligned}
\Lambda_i(\eta) = {} & \lambda_{i1}\left[\cosh(B_j)+\sinh(B_j)\right]+\lambda_{i2}\left[(B_j\cosh(B_j)\right.\\
& \left.-\sinh(B_j))+(B_j\sinh(B_j)-\cosh(B_j))\right]\\
& +\lambda_{i3}[(B_j^2\cosh(B_j)-2B_j\sinh(B_j)+2\cosh(B_j))\\
& +(B_j^2\sinh(B_j)-2B_j\cosh(B_j)+2\sinh(B_j))]\\
& +\lambda_{i4}[\cosh(B_{j+2})+\sinh(B_{j+2})]\\
& +\lambda_{i5}[(B_{j+2}\cosh(B_{j+2})-\sinh(B_{j+2}))\\
& +(B_{j+2}\sinh(B_{j+2})-\cosh(B_{j+2}))]\\
& +\lambda_{i6}[\cosh(B_{j+4})+\sinh(B_{j+4})].
\end{aligned}
$$

$$
\begin{aligned}
&\text{For } i=1 \quad \text{set } j=1, \qquad i=2 \quad \text{set } j=2,\\
&\text{For } i=3 \quad \text{set } j=1, \qquad i=4 \quad \text{set } j=2.
\end{aligned}
\tag{55}
$$

2.3.3. Heat transfer calculations

The wall heat transfer coefficient for the two-equation model is obtained from

$$
h_{w2} = \frac{q_w}{T_w - T_{f,b}} \tag{56}
$$

and the Nusselt number at the channel wall is given by

$$
Nu_{w2} = \frac{h_{w2}D_h}{k_{f,eff}}, \tag{57}
$$

which can be represented as

$$
Nu_{w2} = \frac{-4\gamma^2}{\kappa\theta_{f,b}}, \tag{58}
$$

where the subscript w2 denotes the channel wall for the two-equation model. The non-dimensional fluid bulk mean temperature across the channel cross-section $\theta_{f,b}$ is defined by

$$
\theta_{f,b} = \int_0^1 \theta_f(\eta)\,d\eta. \tag{59}
$$

2.4. One-equation model

The energy equation for the one-equation model case is given by

$$
(\kappa+1)\nabla_\eta^2\theta = u(\xi). \tag{60}
$$

The temperature distribution for the one-equation model is obtained as

$$\theta(\eta)=\frac{1+\Lambda\sqrt{Da}}{\kappa+1}\left[\left(\frac{1}{2}(\eta-1)-\frac{1}{D^2}\left(e^{B_7(\eta)}-e^{B_7(1)}\right)\right)\right.$$
$$+\beta\left(-\frac{1}{2}\eta^2+\frac{1}{D^2}\left(\left(\frac{8}{3}-B_7(\eta)\right)e^{B_7(\eta)}\right.\right.$$
$$\left.+\left(\frac{1}{12}\right)e^{2B_7(\eta)}\right)+\frac{1}{2}-\frac{1}{D^2}\left(\left(\frac{8}{3}-B_7(1)\right)e^{B_7(1)}\right.$$
$$\left.\left.+\left(\frac{1}{12}\right)e^{2B_7(1)}\right)\right)$$
$$+\beta^2\left(\eta^2+\frac{1}{2D^2}\left(\left(\frac{-231}{54}+\frac{B_7(\eta)}{3}+B_7^2(\eta)\right)\frac{e^{B_7(\eta)}}{2}\right.\right.$$
$$\left.-\left(\frac{16}{6}-B_7(\eta)\right)\frac{e^{2B_7(\eta)}}{3}-\left(\frac{1}{54}\right)e^{3B_7(\eta)}\right)\Big)$$
$$-\beta^2\left(1+\frac{1}{2D^2}\left(\left(\frac{-231}{54}+\frac{B_7(1)}{3}+B_7^2(1)\right)\frac{e^{B_7(1)}}{2}\right.\right.$$
$$\left.\left.\left.-\left(\frac{16}{6}-B_7(1)\right)\frac{e^{2B_7(1)}}{3}-\left(\frac{1}{54}\right)e^{3B_7(1)}\right)\right)\right]. \tag{61}$$

The wall heat transfer coefficient for the one-equation model is obtained from

$$h_{w1}=\frac{q_w}{T_w-T_b} \tag{62}$$

and the Nusselt number for the one-equation model is given by

$$Nu_{w1}=\frac{h_{w1}D_h}{k_{f,eff}}, \tag{63}$$

which can be represented as

$$Nu_{w1}=\frac{-4\gamma^2}{\kappa\theta_b}, \tag{64}$$

where the non-dimensional bulk mean temperature across the channel cross-section θ_b for the one-equation model is,

$$\theta_b=\int_0^1\theta(\eta)\,d\eta. \tag{65}$$

2.4.1. Error map

The error in the Nusselt number based on using the one-equation model is found by using the analytical expressions given in Eqs. (59) and (65)

$$E=\frac{Nu_{w1}-Nu_{w2}}{Nu_{w2}}=\frac{\theta_{f,b}}{\theta_b}-1. \tag{66}$$

3. Results and discussion

An in depth description of the physical attributes pertaining to the temperature differential between the fluid and solid phases is given in Lee and Vafai [4] and will not be repeated here. The role of the pertinent parameters and their physical effects are clearly shown in the upcoming figures. The analytical temperature distribution was compared with the numerical solution of the momentum and energy equations for a range of pertinent physical parameters *Bi*, *Da*, Λ and κ as shown in Figs. 2–4. An excellent agreement was found between analytical and numerical results. Variations of the four controlling parameters were used to illustrate their influence on the temperature profile for both the solid and liquid phases. Considering the case for $Da=10^{-2}$, $\Lambda=0$ and a small κ as shown in Fig. 2(a), when *Bi* is small, the temperature difference between the two phases was relatively large due to a small Biot number, thus causing a weak internal heat transfer exchange between the fluid and solid. The small value of κ translate into a small fluid conductivity which result in an uniform temperature near the center of the channel. As the Biot number increases, the internal heat transfer exchange increases, causing the fluid temperature to become closer to the solid temperature which remains almost unchanged, leading to a relatively small temperature difference between the fluid and solid phases.

The effect of an increase in the thermal conductivity ratio, κ, on the fluid and solid temperatures for two different values of *Bi* is shown in Fig. 2(b). Due to a larger fluid conductivity, fluid conduction will become substantial within most of the channel creating a parabolic temperature distribution. A larger Biot number, results in a smaller temperature difference between the two phases. Decreasing the Biot number, causes the solid temperature to become closer to the fluid temperature which hardly changes, resulting in a small temperature difference between the two phases. The fluid conduction which also controlled the heat transfer process for the large κ case results in once again a parabolic profile.

The effect of variations in the inertial parameter on the fluid and solid phases are shown in Figs. 2–4 for various values of *Bi* and κ for $Da=10^{-2}$. As the Inertial parameter increases, the order of magnitude of the temperature difference increases. However, the temperature distribution for both solid and liquid phases follows the same trend.

The present analytical solution based on the generalized flow model for the fluid and solid phases was compared with the analytical solution given by Lee and Vafai [4]. This was done by using a small Darcy number of 10^{-8} and $\Lambda=0$ in the present analytical solution based on the generalized flow model so as to induce a Darcian velocity distribution similar to that considered in Lee and Vafai [4]. Comparisons were done for four sets of Biot number, *Bi*, and ratio of effective fluid to solid conductivity, κ, as shown in

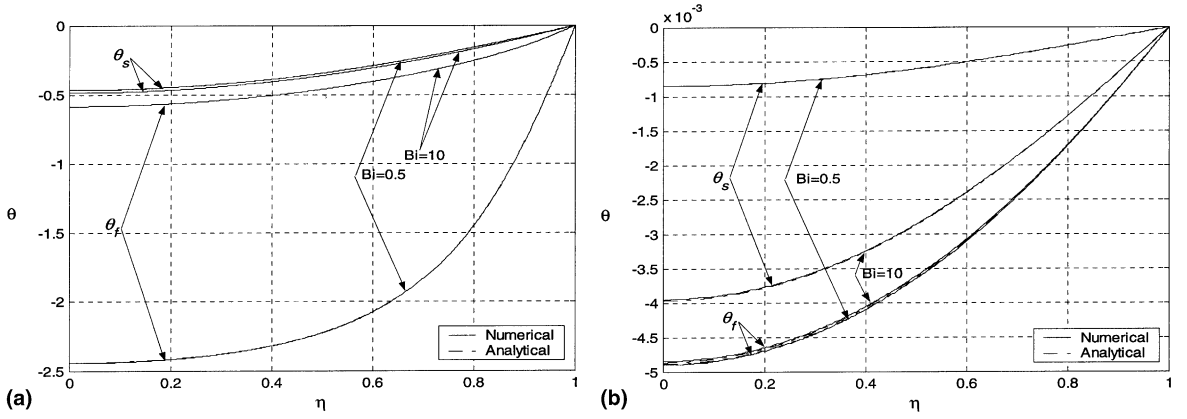

Fig. 2. Comparison of the numerical and analytical temperature distributions for both solid and fluid phases at $Da = 10^{-2}, \Lambda = 0$: (a) $\kappa = 0.01$; (b) $\kappa = 100$.

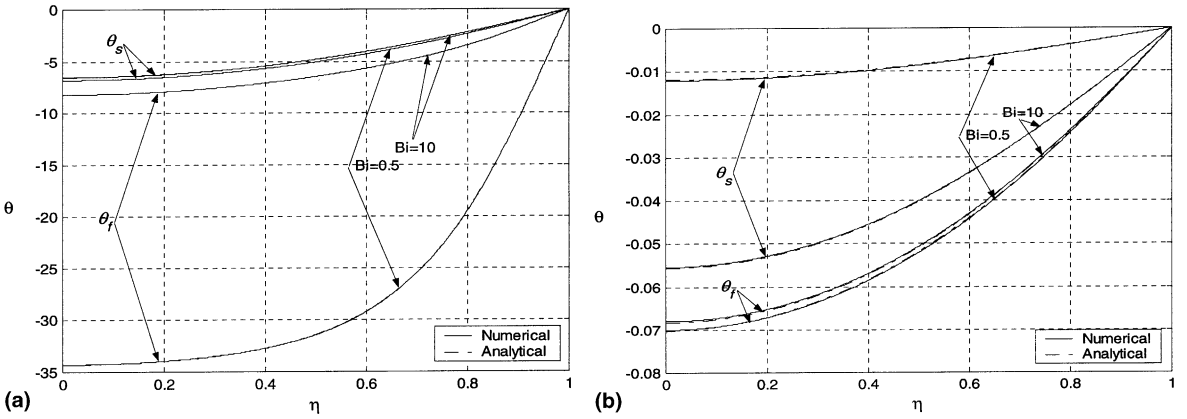

Fig. 3. Comparison of the numerical and analytical temperature distributions for both solid and fluid phases at $Da = 10^{-2}, \Lambda = 10$: (a) $\kappa = 0.01$; (b) $\kappa = 100$.

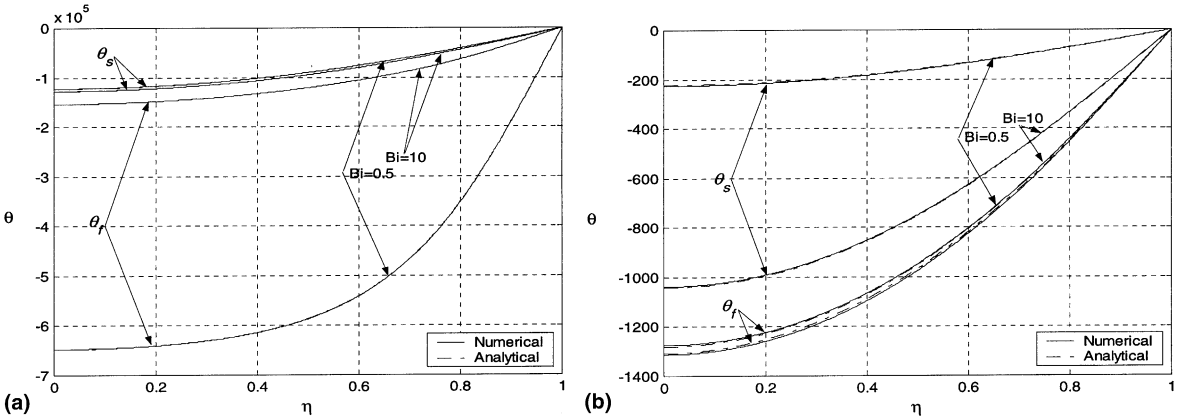

Fig. 4. Comparison of the numerical and analytical temperature distributions for both solid and fluid phases at $Da = 10^{-2}, \Lambda = 100$: (a) $\kappa = 0.01$; (b) $\kappa = 100$.

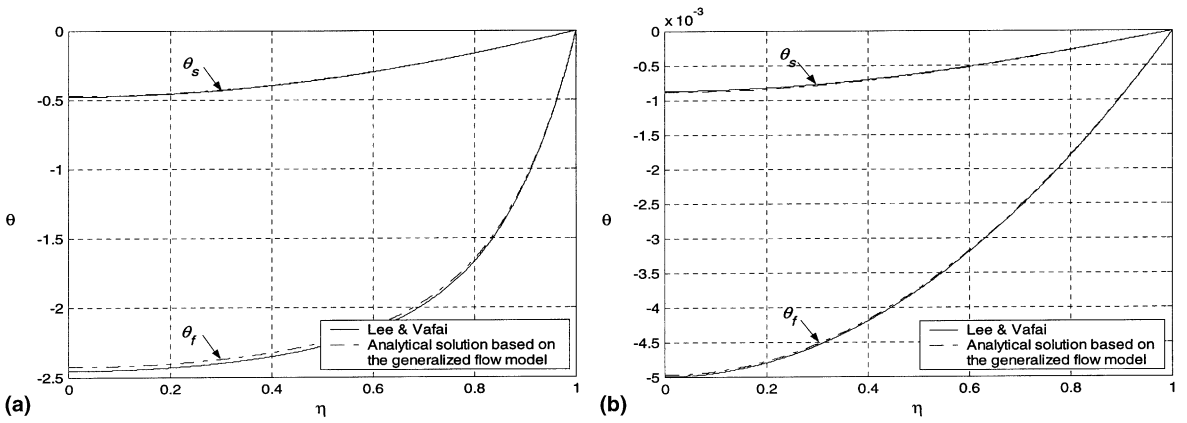

Fig. 5. Solid and fluid phase temperature distribution comparisons between the analytical solution of Lee and Vafai [4] and the present work for $Bi = 0.5$, $Da = 10^{-8}$, $\Lambda = 0$: (a) $\kappa = 0.01$; (b) $\kappa = 100$.

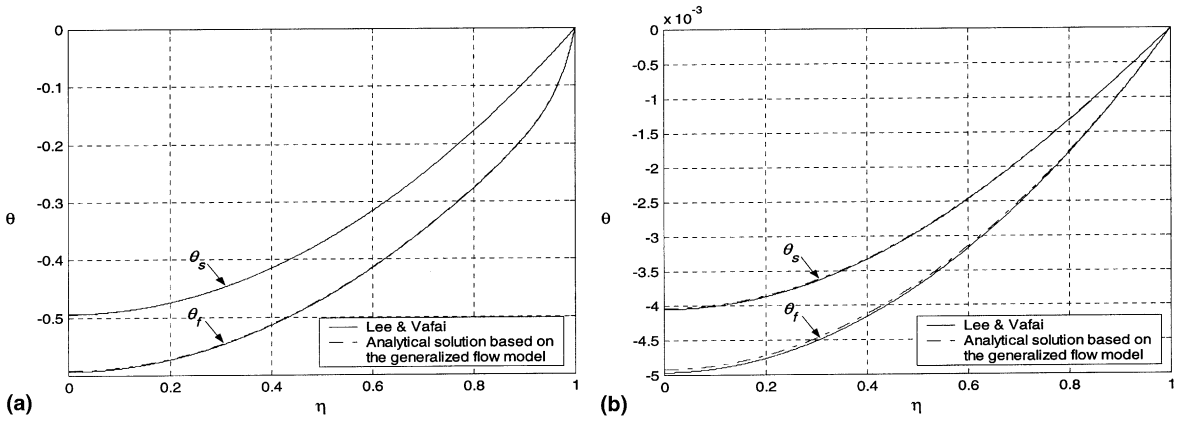

Fig. 6. Solid and fluid phase temperature distribution comparisons between the analytical solution of Lee and Vafai [4] and the present work for $Bi = 10$, $Da = 10^{-8}$, $\Lambda = 0$: (a) $\kappa = 0.01$; (b) $\kappa = 100$.

Figs. 5 and 6. Excellent agreements were found between the two solutions.

Error maps for the validity of the one-equation model for $Da = 10^{-4}$ are shown in Fig. 7. These error maps are based on comparisons between the one- and two-equation model Nusselt numbers as shown in Eq. (67). The numbers displayed on Fig. 7 are indicative of the error incurred in using the one-equation model as opposed to the more general two-equation model. For small values of both controlling parameters Bi and κ, the error maps show an invalid implementation of the one-equation model, while the error decreases as one or both parameters increases as depicted by the error maps in Fig. 7. Figs. 7(a)–(c) demonstrate that as the inertial parameter increases, the error in using one-equation model increases slightly. Fig. 8 displays an error map for a larger Darcy number, $Da = 10^{-2}$. Comparison between the error maps in Fig. 7 and Fig. 8 illustrate that the error decreases as the Darcy number decreases. Overall, the inertial parameter and Darcy number had a substantially smaller influence on establishing the validity of the one-equation model than the Biot number and the thermal conductivity ratio.

4. Conclusions

Forced convective flow through a channel filled with a porous medium was investigated analytically in this work. Energy equations for the solid and fluid phases were used employing a non-thermal equilibrium model and the Brikman–Forchhiemer–extended Darcy model. An analytical representation of the temperature field for both phases was obtained incorporating the effects of Biot number, Darcy number, inertial parameter and the conductivity ratio. The temperature difference

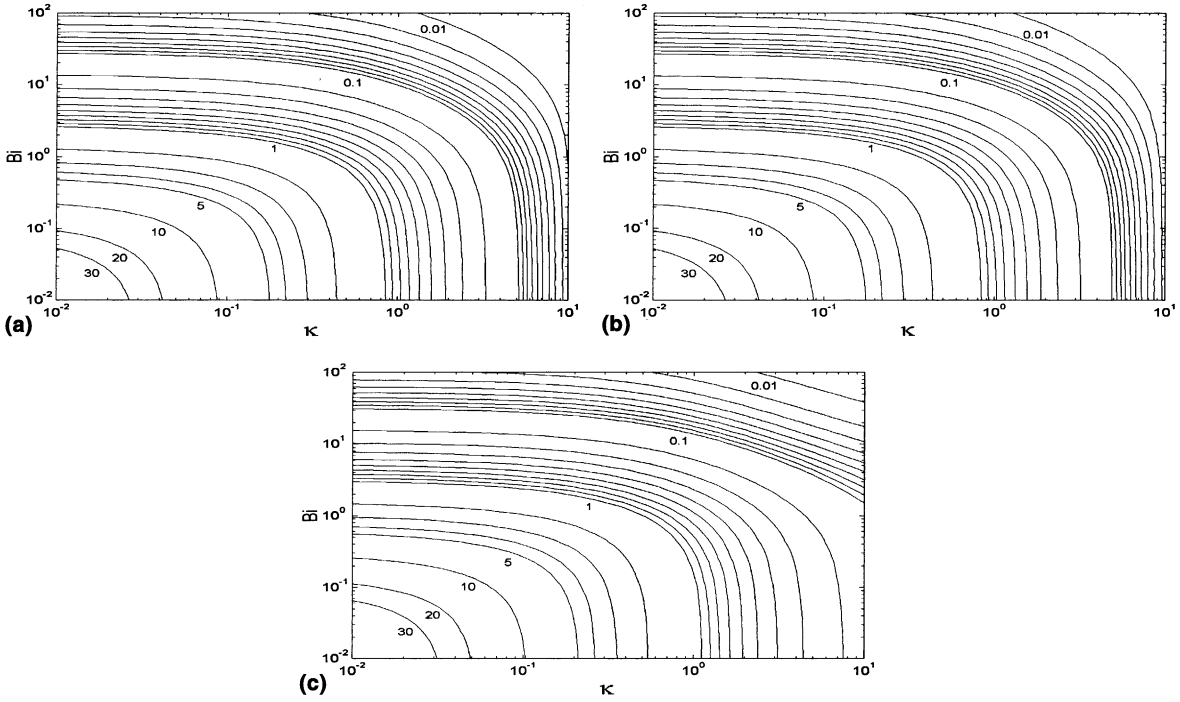

Fig. 7. Error maps for the validity of one-equation model at $Da = 10^{-4}$, (a) $\Lambda = 0$: (b) $\lambda = 10$; (c) $\Lambda = 100$.

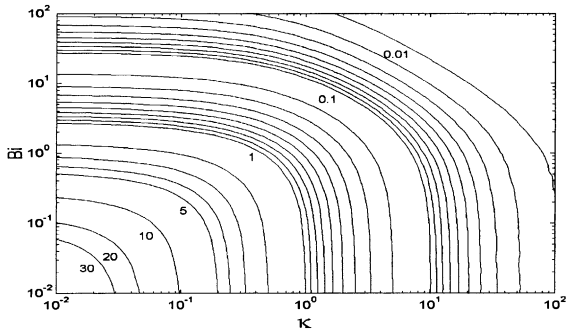

Fig. 8. Error map for the validity of one-equation model at $\Lambda = 10$ and $Da = 10^{-2}$.

between the fluid and solid phases was found to decrease with an increase in the Biot number, *Bi*, due to higher internal convection between the two phases, while an increase in κ resulted in a relative increase in fluid conduction throughout instead of being confined near the channel center. Finally, error maps based on the Nusselt number were obtained to check the validity of the one-equation model for different physical parameters. Smaller values of the Biot number, *Bi*, and the thermal conductivity ratio, κ, resulted in an increase in the error demonstrating a required use of the two-equation model instead of the one-equation model. It was also established that the Darcy number, *Da*, and the inertial parameter, Λ, have a smaller role in determining the validity of the one-equation model as compared to the Biot number, *Bi*, and the thermal conductivity ratio, Λ.

References

[1] K. Vafai, C.L. Tien, Boundary and inertia effects on flow and heat transfer in porous media, Int. J. Heat Mass Transfer 24 (1981) 195–203.

[2] K. Vafai, R. Thiyagaraja, Analysis of flow and heat transfer at the interface region of a porous medium, Int. J. Heat Mass Transfer 30 (1987) 1391–1405.

[3] A. Amiri, K. Vafai, Analysis of dispersion effects and non-thermal equilibrium, non-Darcian, variable porosity, incompressible flow through porous media, Int. J. Heat Mass Transfer 37 (1994) 939–954.

[4] D.Y. Lee, K. Vafai, Analytical characterization and conceptual assessment of solid and fluid temperature differentials in porous media, Int. J. Heat Mass Transfer 42 (1999) 423–435.

[5] S.J. Kim, D. Kim, D.Y. Lee, On the local thermal equilibrium in microchannel heat sinks, Int. J. Heat Mass Transfer 43 (2000) 1735–1748.

[6] K. Vafai, S.J. Kim, Forced convection in a channel filled with a porous medium: an exact solution, J. Heat Transfer 111 (1989) 1103–1106.

[7] A.V. Kuznetsov, Thermal non-equilibrium, non-Darcian forced convection in a channel filled with a fluid saturated

porous medium – a perturbation solution, Appl. Scientific Res. 57 (1997) 119–131.
[8] A. Bejan, Convection Heat Transfer, second ed., Wiley, New York, 1995.
[9] B. Alazimi, K. Vafai, Analysis of variants within the porous media transport models, ASME J. Heat Transfer 122 (2000) 303–326.